

## Integrated Backward Second-Harmonic Generation through Optically Induced Quasi-Phase-Matching

Ozan Yakar<sup>✉</sup>, Edgars Nitiss, Jianqi Hu<sup>✉</sup>, and Camille-Sophie Brès<sup>✉\*</sup>

École Polytechnique Fédérale de Lausanne (EPFL), Photonic Systems Laboratory (PHOSL), Lausanne CH-1015, Switzerland



(Received 9 February 2023; accepted 28 August 2023; published 5 October 2023)

Quasi-phase-matching for efficient backward second-harmonic generation requires sub- $\mu\text{m}$  poling periods, a nontrivial fabrication feat. For the first time, we report integrated first-order quasiphase-matched backward second-harmonic generation enabled by seeded all-optical poling. The self-organized grating inscription circumvents all fabrication challenges. We compare backward and forward processes and explain how grating period influences the conversion efficiency. These results showcase unique properties of the coherent photogalvanic effect and how it can bring new nonlinear functionalities to integrated photonics.

DOI: [10.1103/PhysRevLett.131.143802](https://doi.org/10.1103/PhysRevLett.131.143802)

The efficiency of nonlinear wave mixing processes is clamped by the mismatch of momenta due to dispersion. Quasi-phase-matching (QPM) [1] is a technique used to compensate the momentum mismatch and recover the efficiency of the parametric conversion through the periodic reversal of nonlinear susceptibility in the medium. Integrated waveguiding structures are ideal candidates for nonlinear optical processes as they offer added flexibility for dispersion engineering, higher light intensities under reduced power, and access to a wide range of materials. In integrated platforms, QPM has been realized by domain inversion in lithium niobate on insulator ferroelectric waveguides through electric-field poling [2], with p-n junctions in silicon [3], or by optically inducing a periodic electric field by all-optical poling (AOP) enabled by the coherent photogalvanic effect. AOP, first extensively studied in optical fibers [4–9], was recently demonstrated in both silicon nitride ( $\text{Si}_3\text{N}_4$ ) waveguides [10–12] and microresonators [13–15]. During AOP, multiphoton absorption interference leads to the inscription of periodic dc field automatically satisfying QPM condition for the participating waves. The obtained QPM grating and effective second-order susceptibility  $[\chi^{(2)}]$  overcome the typical trade-off between device functionality and performance and fabrication complexity. This effective  $\chi^{(2)}$  brings added functionalities to  $\text{Si}_3\text{N}_4$ , an already mature linear platform with its low loss and high damage threshold [16,17] and heavily exploited for third-order  $[\chi^{(3)}]$  nonlinear effects [18–22]. High level of second-harmonic (SH) powers

commensurate with those obtained in typical  $\chi^{(2)}$  platforms can be obtained by leveraging the robustness and high power handling capability of  $\text{Si}_3\text{N}_4$ . As such, the demonstration of broadband second-harmonic generation (SHG) [12,23], difference-frequency generation [24] and spontaneous parametric down-conversion [25] were reported in  $\text{Si}_3\text{N}_4$  waveguides.

Most of the QPM work, in any platform, has been devoted to forward second-harmonic generation (FSHG), where the pump and generated SH propagates in the same direction [Fig. 1(a)]. The required QPM period,  $\Lambda_{\text{FSHG}}$  is determined by the momentum mismatch between the pump and its SH given by  $\Lambda_{\text{FSHG}} = 2\pi/\Delta k = \lambda/(2|n_{2\omega} - n_{\omega}|)$ , where  $\Delta k$  is the difference in wave vectors,  $\lambda$  is the pump wavelength,  $n_{2\omega}$  and  $n_{\omega}$  are the effective indices at the SH and pump, respectively. Typically the necessary periods, in both crystals and waveguides, are on the order of a few microns. The fabrication of external structures of such dimensions, as required for electric-field poling, is possible. However, submicron QPM periods necessary for mirrorless optical parametric oscillators [26], spontaneous parametric down-conversion with very narrow spectrum [27,28], or backward second-harmonic generation (BSHG) [29], where the pump and SH waves travel in opposite directions [Fig. 1(b)], face significant fabrication challenges [30,31]. As such, while BSHG has been studied theoretically for several configurations [32,33], there have been limited experimental demonstrations. BSHG has been achieved in bulk materials such as periodically poled lithium niobate [34] and potassium titanyl phosphate (KTP) using high-order QPM [35–37], or stacked metasurfaces [38] with first-order QPM. There is also a continuous effort to achieve BSHG in integrated photonics. Current demonstrations include using plasmonic structures

Published by the American Physical Society under the terms of the [Creative Commons Attribution 4.0 International license](https://creativecommons.org/licenses/by/4.0/). Further distribution of this work must maintain attribution to the author(s) and the published article's title, journal citation, and DOI.

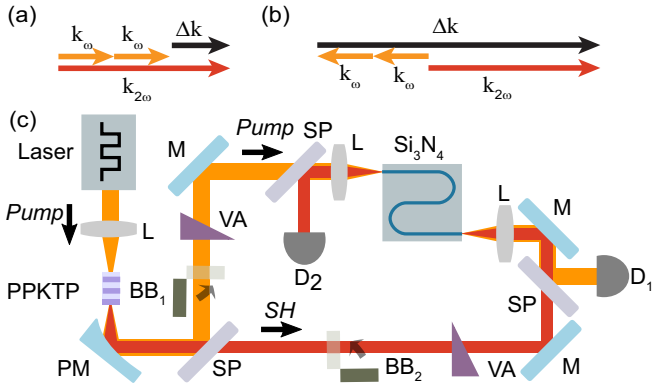


FIG. 1. Illustration of momentum conservation of the (a) forward and (b) backward SHG processes. (c) AOP setup for inducing BSHG QPM. Pulsed light is sent to PPKTP after which pump and seed SH are collimated in the parabolic mirror. Pump and SH are split and coupled through opposite ends of the waveguide, with their path lengths matched.  $BB_{1,2}$ , beam block for pump and SH, respectively; VA, variable attenuator; M, mirror; SP, short-pass dichroic mirror (cutoff at 1100 nm); L, lens; PM, parabolic mirror;  $D_{1,2}$ , detector.

with negative refractive index materials relying on perfect phase matching [39,40]. Nevertheless, these techniques face challenges related to fabrication constraints, which limit efficiency due to the tolerances and hinder the ability to replicate small structures. Moreover, they necessitate high power levels given the large beam sizes. Furthermore, plasmonic structures suffer from significant optical losses.

In this Letter, for the first time, we demonstrate AOP induced first-order QPM gratings with submicron periods [ $\Lambda_{\text{BSHG}} = \lambda / (2|n_{2\omega} + n_{\omega}|)$ , see Fig. 1(b)] enabling BSHG with on-chip conversion efficiency (CE), defined as  $\eta_{2\omega} = P_{2\omega} / P_{\omega}^2$ , of  $1.2 \times 10^{-4} \%$ /W, which in the C band is comparable with the highest CE value reached in any platform [34]. We achieve this by leveraging the self-organization properties of the optically written gratings, and by seeding the AOP process with counterpropagating coherent pump and SH seed light, bypassing the complex fabrication steps utilized in other platforms. We confirm that BSHG allows for narrow bandwidth SHG as well as very high thermal sensitivity compared to its bandwidth. We also explain how the grating period values affect the achievable CE.

The AOP process results in a grating with a periodicity of  $\chi^{(2)}$  automatically compensating the wave vector mismatch of the interfering coherent waves responsible for the effect. During the process, photogalvanic current ( $j_{\text{ph}}$ ), proportional to  $(E_{\omega}^*)^2 E_{2\omega} e^{i\Delta k z} + \text{c.c.}$ , leads to charge separation and therefore inscription of a dc electric field with periodic modulation satisfying QPM condition. Here,  $E_{\omega}$  and  $E_{2\omega}$  are the complex electric field amplitudes of pump and SH fields, respectively,  $z$  is the propagation distance,  $*$  and c.c. denote complex conjugate,  $\Delta k$  is the difference of the wave vectors of pump and SH [Figs. 1(a) and 1(b)]. The inscribed

field saturates due to photoconductivity ( $\sigma$ ). As such, FSHG can be obtained by solely launching a pump wave in a waveguide or by a seeded process [41,42] where both the pump and its SH are simultaneously coupled to the waveguide. By injecting the pump and its SH from opposite sides of the waveguide, a QPM grating for BSHG could therefore be optically inscribed. The experimental setup for poling using two counterpropagating beams is shown in Fig. 1(c). We carried out the demonstration in an integrated  $\text{Si}_3\text{N}_4$  waveguide buried in  $\text{SiO}_2$  fabricated by LIGENTEC SA using its AN800 platform. The waveguide has a cross section of  $1.3 \mu\text{m} \times 0.8 \mu\text{m}$  and is folded in nine meanders for a total length of 4.3 cm, including input and output tapers. Backward-seeded AOP is initiated by 1550 nm light together with its SH, externally generated using a nonlinear crystal: periodically poled KTP (PPKTP). The 1550 nm pump was first shaped into a 5 ns pulse train at 1 MHz repetition rate and was amplified to reach peak power up to 8.6 W in the waveguide. The pump and its SH are collimated by a parabolic mirror, split and coupled through opposite ends of the waveguide in transverse electric polarization. The power of both the forward pump and the backward SH seed can be controlled using variable attenuators. During this process, the optical path lengths are matched in order to ensure the overlap of pump and seed SH pulses inside the waveguide, as to enable grating inscription. It should be noted that the pulses, when not temporally overlapping inside the waveguide, can contribute to grating erasure. In our case we estimate that the inscription-to-erasure time ratio is around 35:1. The forward pump is monitored by detector  $D_1$  while SH is collected by detector  $D_2$  after a dichroic mirror. Initially, seeding SH is blocked with a beam block ( $BB_2$ ) and no backward SH is observed. During seeded AOP,  $BB_2$  is kept open, and is occasionally shut for a short period of time as to record the dynamic evolution of BSHG in the waveguide. Once saturation is reached, the performance of the device such as maximum backward second-harmonic CE and QPM bandwidth is quantified using cw pump light.

The poling traces for three different SH powers and constant pump power of 8.6 W are presented in Fig. 2(a). First, we clearly measure SH being generated backward. Second, the initial growth rate ( $d\eta_{2\omega}/dt|_{t=0}$ ) increases with seed SH power. While the maximum CE also initially increases, it eventually saturates owing to the enhanced  $\sigma$  [42]. Evidently, the resulting CEs for BSHG are close to 2 orders of magnitude lower than for FSHG when similar pump and SH seed power levels are used. The main factor controlling the efficiency of AOP is the initial growth rate, which correlates to how the current is translated to the electric field. Compared to forward AOP,  $d\eta_{2\omega}/dt|_{t=0}$ , numerically fitted following high-seed approximation [42], is here found to be close to 100 times less. This is explained by the small grating period and the closeness of the separated charges, leading to screening. As a

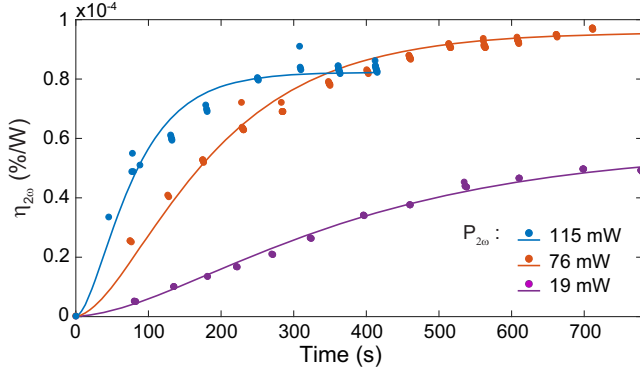


FIG. 2. Experimental BSHG CE during AOP (dotted) and fit (solid line) according to Ref. [42] for a constant peak pump power of 8.6 W and varying peak SH seed power inside the waveguide. There is a 9% error in the CE measurements due to the sum of errors in detectors.

consequence, the electric field is weaker and the growth rate is reduced compared to larger grating periods even under identical photogalvanic current. Using Eq. (S21) in

$$E_y(\Delta k; x, y, z) = \frac{2\Delta k \cos(\Delta kz)}{4\pi\epsilon} \iint dx' dy' \rho(x' + x, y' + y) y \frac{K_1(\Delta k \sqrt{x^2 + y^2})}{\sqrt{x^2 + y^2}}, \quad (1)$$

where  $K_1$  is the first-order modified Bessel function of the second kind (see Supplemental Material, Sec. 1). As  $K_1$  is an exponentially decaying function,  $E_y$  will decay with increasing  $\Delta k$ , namely, with decreasing grating period. This is due to the screening of electric fields. The effect of the period on the achievable electric fields was simulated using COMSOL MULTIPHYSICS software for a charge

Supplemental Material [43], Sec. 3, the simulated initial growth rate with respect to the grating period is shown in Fig. S1. It can be seen that the initial growth rate is reduced by approximately 10 times for backward-wave SHG (when the two pump photons propagate in different directions) and 100 times for BSHG due to the screening of charges.

To confirm the behavior of the electric field as a function of the grating period, without loss of generality, let us assume that within the waveguide there is an equal number of mobile positive charge carriers and immobile negative charge carriers evenly distributed [44]. After AOP the positive mobile charge carrier density inside the waveguide can be described as  $\rho(x, y, z) = \rho(x, y) \cos(\Delta kz) + \rho_0(x, y, z)$  where  $\rho_0$  is constant. While the total number of charges in the waveguide does not change, the separated charge carriers lead to an induced local electric field. Hence, it can be observed that  $\iint dx dy \rho(x, y) = 0$  as the charges are generated in pairs of opposite signs. Using Coulomb's law, the  $y$  component of the electric field ( $E_y$ ) at an arbitrary position  $(x, y, z)$  becomes

distribution of  $C = C_{\text{bulk}}[1 + ye^{-y^2/\gamma^2} \cos(\Delta kz)]$  using the material constants and physical model described in Ref. [45]. We showcase simulation results for two specific cases with periodicity  $\Lambda$  of charge spatial modulation being  $6 \mu\text{m}$  and  $0.2 \mu\text{m}$ . Gratings with such period can satisfy the QPM condition for FSHG and BSHG, respectively, as will be shown below. In Figs. 3(a)–3(c) the simulated charge

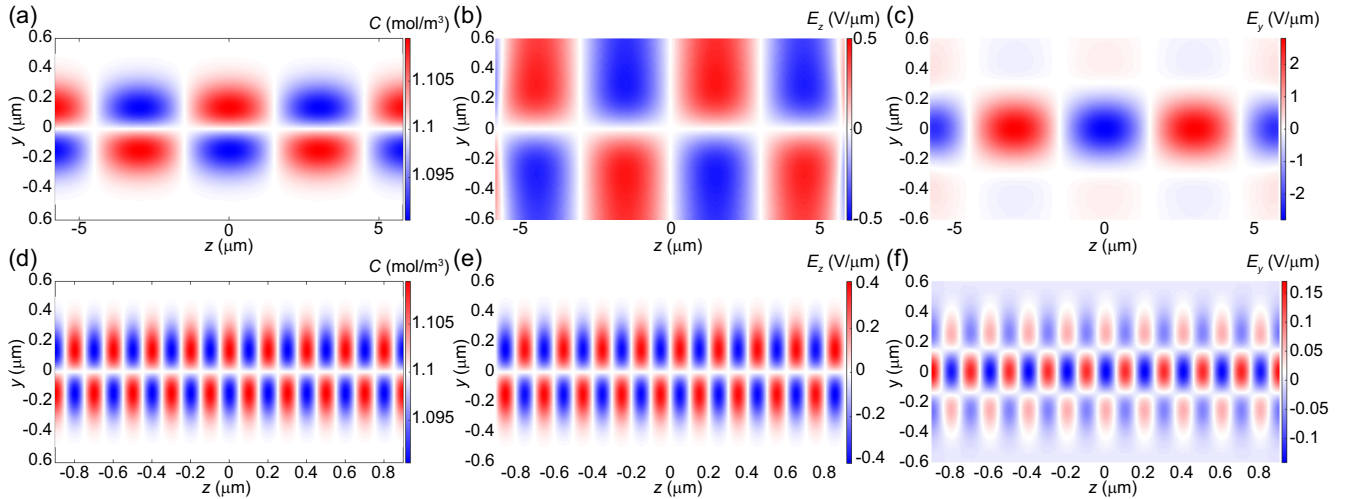


FIG. 3. The effect of poling period on the inscribed dc electric field is shown. A periodically oscillating charge concentration along the waveguide  $C$  (related to charge density  $\rho = qN_A C$ , where  $q$  is the electronic charge [44] and  $N_A$  is the Avogadro constant) and resulting longitudinal ( $E_z$ ) and transverse ( $E_y$ ) components of the electric field are simulated for a period  $6 \mu\text{m}$  (a)–(c) and  $0.2 \mu\text{m}$  (d)–(f), respectively.

distribution  $C$ , longitudinal electric field  $E_z$ , and transverse electric field  $E_y$  are shown for the case when  $\Lambda = 6 \mu\text{m}$ . It is important to note that the transverse field strength  $E_y$  determines the effective second-order nonlinearity  $\chi_{\text{eff}}^{(2)}$  and, hence the CE. In Figs. 3(d)–3(f) we also display the  $C$ ,  $E_z$  and  $E_y$  with  $\Lambda = 0.2 \mu\text{m}$ . By comparing the  $E_y$  in both cases, it can be recognized that the magnitude of  $E_y$  reduces approximately tenfold because of screening when the period is decreased from  $6 \mu\text{m}$  to  $0.2 \mu\text{m}$ . Notably, the longitudinal field  $E_z$  is almost the same for both cases as can be seen from Figs. 3(b) and 3(e).

We measure the CE spectrum for both backward and forward directions. After AOP, if the propagation loss is ignored, the CE for BSHG becomes [42]

$$\eta_{2\omega} \approx \frac{(\omega\chi_{\text{eff}}^{(2)}L)^2}{2c^3\epsilon_0\bar{n}^2\bar{S}} \text{sinc}^2\left(\left(\Delta k - \frac{2\pi}{\Lambda}\right)\frac{L}{2}\right), \quad (2)$$

where  $\Delta k(\lambda) - (2\pi/\Lambda)$  is the net wave vector mismatch after AOP,  $L$  is the grating length,  $\bar{n} = (n_{\omega}^2 n_{2\omega})^{1/3}$  with  $n_{q\omega}$  being the effective refractive index at frequency  $q\omega$  ( $q = 1, 2$ ),  $\bar{S} = (S_{\omega}^2 S_{2\omega})^{1/3}$  is the effective area, where  $S_{q\omega} = (\iint dx dy |E_{q\omega}|^2)^{3/2} / (\iint dx dy |E_{q\omega}|^6)^{1/2}$ ,  $\chi_{\text{eff}}^{(2)}$  is the effective second-order nonlinearity, and  $\text{sinc}(x) = \sin(x)/x$ . The experimental data and the fits using Eq. (2) are shown in Fig. 4(a). Here, the effective area and effective refractive index data used for fitting are obtained using finite element method simulations. We clearly see that forward SH is not generated while BSHG occurs with a very narrow bandwidth of 7.2 pm and a peak efficiency estimated around  $1.2 \times 10^{-4}\%/W$ . This is in stark contrast to FSHG in the same waveguide after forward poling [see Fig. 1(a) inset], which results in a much broader bandwidth of 3 nm. The ultranarrow bandwidths arise in BSHG because the pump and the second harmonic wave, which travel in opposite directions, experience a significant group velocity mismatch. From the fit of the backward AOP CE spectrum, we extract the grating period,  $\chi_{\text{eff}}^{(2)}$  and grating length to be 206.3 nm,  $1.46 \times 10^{-3} \text{ pm/V}$  and 3.5 cm (81% of the waveguide length), respectively. As seen from Fig. 4(b) the steady state bandwidth is constant over different seeding conditions, which well agrees with Eq. (2).

The position of the CE peak can be thermally tuned [46,47], which for BSHG, becomes

$$\frac{\Delta\lambda}{\delta\lambda_{\text{FWHM}}} \approx \frac{\partial n_{\text{eff}}'}{\partial T} \frac{Lc}{0.44\lambda_0^2} \Delta T, \quad (3)$$

where  $n_{\text{eff}}' = n_{\omega} + n_{2\omega}$ ,  $\Delta T$  is the variation in temperature,  $\Delta\lambda$  is the resulting detuning in wavelength, and  $\delta\lambda_{\text{FWHM}}$  is the full-width half-maximum (FWHM) of QPM spectra. We experimentally investigate the thermal sensitivity of BSHG as shown in Fig. 4(c) by varying the chip

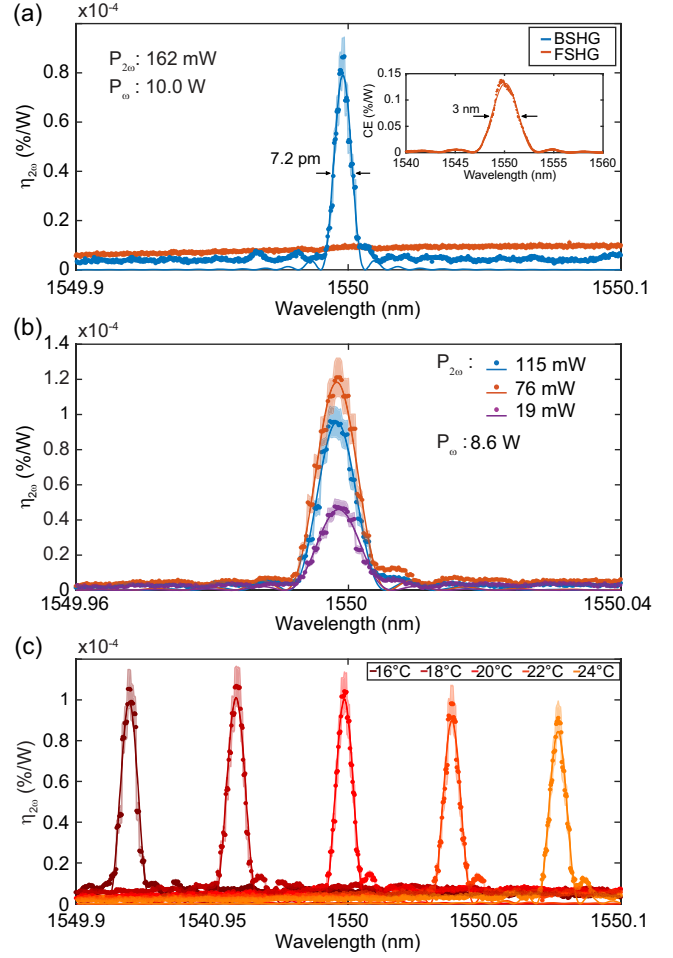


FIG. 4. (a) Experimental BSHG CE spectrum (blue dots) and its sinc-squared fit using Eq. (2) (blue solid line) FSHG CE spectrum shown in red for backward poling. Inset: FSHG CE spectrum of forward poling. (b) CE spectra are shown for different SH seed powers. The steady state bandwidths are approximately identical for different seed powers. (c) CE spectra (dots, experimental data; solid lines, sinc-squared fits) for temperatures from 16°C to 24°C. The waveguide was initially poled at 1550 nm and 20°C. The shaded areas cover the possible error due to the measurement error of the detectors.

temperature. We extract the thermal shift of the QPM peak to be 19 pm/°C. It can be seen that it is extremely sensitive compared to its bandwidth.

In conclusion, seeded AOP represents a straightforward way to induce exceptionally short-period QPM gratings that can satisfy BSHG in integrated platforms. Seeded AOP circumvents fabrication challenges of the standard electrical poling techniques for implementation of submicron nonlinear gratings, while the self-organized QPM grating results in a near perfect match between experimental and theoretical spectral response. As predicted by the theory, we observe that only the nonlinear grating strength changes with changing seeding conditions. The poled waveguides show extremely narrow QPM spectra, highly tunable with

temperature, with CE of  $1.2 \times 10^{-4}\%$ /W, comparable to the highest one achieved in C band so far [34]. Apart from efficiency, optical poling of  $\text{Si}_3\text{N}_4$  demonstrates a better performance regarding the losses, reconfigurability, control in dispersion, and ease of operation. This demonstration paves the way for the realization of theoretically proposed effects such as phase conjugation [48], pulse shaping [32], self-pulsing [29], and bistability [49] through second-order nonlinearity. We theoretically explain the reduction of efficiencies compared to FSHG due to the screening of electric fields with submicron periods. The efficiency could be improved by using longer waveguides, exploiting other materials such as silicon-rich silicon nitride or using structures like Bragg gratings to separate the charges further.

This work was supported by ERC grant PISSARRO (ERC-2017-CoG 771647). The samples used for the experiment were fabricated by LIGENTEC SA. O. Y. would like to thank Dr. Christian Lafforgue and Mr. Serhat Bakırtaş for valuable discussions.

\*Corresponding author: [camille.bres@epfl.ch](mailto:camille.bres@epfl.ch)

- [1] J. A. Armstrong, N. Bloembergen, J. Ducuing, and P. S. Pershan, Interactions between light waves in a nonlinear dielectric, *Phys. Rev.* **127**, 1918 (1962).
- [2] C. Wang, C. Langrock, A. Marandi, M. Jankowski, M. Zhang, B. Desiatov, M. M. Fejer, and M. Lončar, Ultrahigh-efficiency wavelength conversion in nanophotonic periodically poled lithium niobate waveguides, *Optica* **5**, 1438 (2018).
- [3] E. Timurdogan, C. V. Poulton, M. Byrd, and M. Watts, Electric field-induced second-order nonlinear optical effects in silicon waveguides, *Nat. Photonics* **11**, 200 (2017).
- [4] U. Österberg and W. Margulis, Dye laser pumped by nd: Yag laser pulses frequency doubled in a glass optical fiber, *Opt. Lett.* **11**, 516 (1986).
- [5] E. Baskin and M. Entin, Coherent photovoltaic effect due to the quantum corrections, *Sov. J. Exp. Theor. Phys. Lett.* **48**, 601 (1988), [http://www.jetpletters.ru/ps/1110/article\\_16792.shtml](http://www.jetpletters.ru/ps/1110/article_16792.shtml).
- [6] B. Y. Zel'Dovich and A. Chudinov, Interference of fields with frequencies  $\omega$  and  $2\omega$  in external photoelectric effect, *Sov. J. Exp. Theor. Phys. Lett.* **50**, 439 (1989), [http://www.jetpletters.ru/ps/1133/article\\_17142.shtml](http://www.jetpletters.ru/ps/1133/article_17142.shtml).
- [7] D. Z. Anderson, V. Mizrahi, and J. E. Sipe, Model for second-harmonic generation in glass optical fibers based on asymmetric photoelectron emission from defect sites, *Opt. Lett.* **16**, 796 (1991).
- [8] W. Margulis, F. Laurell, and B. Lesche, Imaging the nonlinear grating in frequency-doubling fibres, *Nature (London)* **378**, 699 (1995).
- [9] E. M. Dianov and D. S. Starodubov, Photoinduced generation of the second harmonic in centrosymmetric media, *Quantum Electron.* **25**, 395 (1995).
- [10] A. Billat, D. Grassani, M. H. Pfeiffer, S. Kharitonov, T. J. Kippenberg, and C.-S. Brès, Large second harmonic generation enhancement in  $\text{Si}_3\text{N}_4$  waveguides by all-optically induced quasi-phase-matching, *Nat. Commun.* **8**, 1016 (2017).
- [11] M. A. Porcel, J. Mak, C. Taballione, V. K. Schermerhorn, J. P. Epping, P. J. van der Slot, and K.-J. Boller, Photo-induced second-order nonlinearity in stoichiometric silicon nitride waveguides, *Opt. Express* **25**, 33143 (2017).
- [12] D. D. Hickstein, D. R. Carlson, H. Mundoor, J. B. Khurgin, K. Srinivasan, D. Westly, A. Kowligy, I. I. Smalyukh, S. A. Diddams, and S. B. Papp, Self-organized nonlinear gratings for ultrafast nanophotonics, *Nat. Photonics* **13**, 494 (2019).
- [13] X. Lu, G. Moille, A. Rao, D. A. Westly, and K. Srinivasan, Efficient photoinduced second-harmonic generation in silicon nitride photonics, *Nat. Photonics* **15**, 131 (2021).
- [14] E. Nitiss, J. Hu, A. Stroganov, and C.-S. Brès, Optically reconfigurable quasi-phase-matching in silicon nitride microresonators, *Nat. Photonics* **16**, 134 (2022).
- [15] J. Hu, E. Nitiss, J. He, J. Liu, O. Yakar, W. Weng, T. J. Kippenberg, and C.-S. Brès, Photo-induced cascaded harmonic and comb generation in silicon nitride microresonators, *Sci. Adv.* **8**, eadd8252 (2022).
- [16] E. Nitiss, T. Liu, D. Grassani, M. Pfeiffer, T. J. Kippenberg, and C.-S. Brès, Formation rules and dynamics of photo-induced  $\chi^{(2)}$  gratings in silicon nitride waveguides, *ACS Photonics* **7**, 147 (2019).
- [17] H. El Dirani, L. Youssef, C. Petit-Etienne, S. Kerdiles, P. Grosse, C. Monat, E. Pargon, and C. Sciancalepore, Ultra-low-loss tightly confining  $\text{Si}_3\text{N}_4$  waveguides and high-q microresonators, *Opt. Express* **27**, 30726 (2019).
- [18] Z. Ye, P. Zhao, K. Twayana, M. Karlsson, V. Torres-Company, and P. A. Andrekson, Overcoming the quantum limit of optical amplification in monolithic waveguides, *Sci. Adv.* **7**, eabi8150 (2021).
- [19] A. Ayan, F. Mazeas, J. Liu, T. J. Kippenberg, and C.-S. Brès, Polarization selective ultra-broadband wavelength conversion in silicon nitride waveguides, *Opt. Express* **30**, 4342 (2022).
- [20] J. S. Levy, M. A. Foster, A. L. Gaeta, and M. Lipson, Harmonic generation in silicon nitride ring resonators, *Opt. Express* **19**, 11415 (2011).
- [21] D. Grassani, E. Tagkoudi, H. Guo, C. Herkommer, F. Yang, T. J. Kippenberg, and C.-S. Brès, Mid infrared gas spectroscopy using efficient fiber laser driven photonic chip-based supercontinuum, *Nat. Commun.* **10**, 1553 (2019).
- [22] T. J. Kippenberg, A. L. Gaeta, M. Lipson, and M. L. Gorodetsky, Dissipative Kerr solitons in optical microresonators, *Science* **361**, eaan8083 (2018).
- [23] E. Nitiss, B. Zabelich, O. Yakar, J. Liu, R. N. Wang, T. J. Kippenberg, and C.-S. Brès, Broadband quasi-phase-matching in dispersion-engineered all-optically poled silicon nitride waveguides, *Photonics Res.* **8**, 1475 (2020).
- [24] E. Sahin, B. Zabelich, O. Yakar, E. Nitiss, J. Liu, R. N. Wang, T. J. Kippenberg, and C.-S. Brès, Difference-frequency generation in optically poled silicon nitride waveguides, *Nanophotonics* **10**, 1923 (2021).
- [25] R. Dalidet, F. Mazeas, E. Nitiss, O. Yakar, A. Stroganov, S. Tanzilli, L. Labonté, and C.-S. Brès, Near perfect two-photon interference out of a down-converter on a silicon photonic chip, *Opt. Express* **30**, 11298 (2022).
- [26] C. Canalas and V. Pasiskevicius, Mirrorless optical parametric oscillator, *Nat. Photonics* **1**, 459 (2007).

- [27] K.-H. Luo, V. Ansari, M. Massaro, M. Santandrea, C. Eigner, R. Ricken, H. Herrmann, and C. Silberhorn, Counter-propagating photon pair generation in a nonlinear waveguide, *Opt. Express* **28**, 3215 (2020).
- [28] Y.-C. Liu, D.-J. Guo, K.-Q. Ren, R. Yang, M. Shang, W. Zhou, X. Li, C.-W. Sun, P. Xu, Z. Xie *et al.*, Observation of frequency-uncorrelated photon pairs generated by counter-propagating spontaneous parametric down-conversion, *Sci. Rep.* **11**, 12628 (2021).
- [29] G. D'Alessandro, P. S. J. Russell, and A. A. Wheeler, Non-linear dynamics of a backward quasi-phase-matched second-harmonic generator, *Phys. Rev. A* **55**, 3211 (1997).
- [30] A. Boes, L. Chang, T. Nguyen, G. Ren, J. Bowers, and A. Mitchell, Efficient second harmonic generation in lithium niobate on insulator waveguides and its pitfalls, *J. Phys.* **3**, 012008 (2021).
- [31] I. Krasnokutska, J.-L. J. Tambasco, and A. Peruzzo, Sub-micron domain engineering in periodically poled lithium niobate on insulator, [arXiv:2108.10839](https://arxiv.org/abs/2108.10839).
- [32] M. Conforti, C. De Angelis, U. K. Sapaev, and G. Assanto, Pulse shaping via backward second harmonic generation, *Opt. Express* **16**, 2115 (2008).
- [33] R. Iliiew, C. Etrich, T. Pertsch, F. Lederer, and Y. S. Kivshar, Huge enhancement of backward second-harmonic generation with slow light in photonic crystals, *Phys. Rev. A* **81**, 023820 (2010).
- [34] A. C. Busacca, S. Stivala, L. Curcio, A. Tomasino, and G. Assanto, Backward frequency doubling of near infrared picosecond pulses, *Opt. Express* **22**, 7544 (2014).
- [35] X. Gu, M. Makarov, Y. J. Ding, J. B. Khurgin, and W. P. Risk, Backward second-harmonic and third-harmonic generation in a periodically poled potassium titanyl phosphate waveguide, *Opt. Lett.* **24**, 127 (1999).
- [36] C. Canalias, V. Pasiskevicius, M. Fokine, and F. Laurell, Backward quasi-phase-matched second-harmonic generation in submicrometer periodically poled flux-grown  $\text{KTiOPO}_4$ , *Appl. Phys. Lett.* **86**, 181105 (2005).
- [37] P. Mutter, K. M. Mølster, A. Zukauskas, V. Pasiskevicius, and C. Canalias, Third order backward second-harmonic generation in periodically poled Rb-doped KTP with a period of 317 nm, in *Conference on Lasers and Electro-Optics* (Optica Publishing Group, San Jose, CA, 2022), p. SM2O.4.
- [38] T. Stolt, J. Kim, S. Héron, A. Vesala, Y. Yang, J. Mun, M. Kim, M. J. Huttunen, R. Czaplicki, M. Kauranen, J. Rho, and P. Genevet, Backward Phase-Matched Second-Harmonic Generation from Stacked Metasurfaces, *Phys. Rev. Lett.* **126**, 033901 (2021).
- [39] S. Lan, L. Kang, D. T. Schoen, S. P. Rodrigues, Y. Cui, M. L. Brongersma, and W. Cai, Backward phase-matching for nonlinear optical generation in negative-index materials, *Nat. Mater.* **14**, 807 (2015).
- [40] L. Liu, L. Wu, J. Zhang, Z. Li, B. Zhang, and Y. Luo, Backward phase matching for second harmonic generation in negative-index conformal surface plasmonic metamaterials, *Adv. Sci.* **5**, 1800661 (2018).
- [41] D. M. Krol, M. M. Broer, K. T. Nelson, R. H. Stolen, H. W. K. Tom, and W. Pleibel, Seeded second-harmonic generation in optical fibers: The effect of phase fluctuations, *Opt. Lett.* **16**, 211 (1991).
- [42] O. Yakar, E. Nitiss, J. Hu, and C.-S. Brès, Generalized coherent photogalvanic effect in coherently seeded waveguides, *Laser Photonics Rev.* **16**, 2200294 (2022).
- [43] See Supplemental Material at <http://link.aps.org/supplemental/10.1103/PhysRevLett.131.143802> for additional information regarding the theoretical description of backward second-harmonic generation and comparison of backward and forward second-harmonic generation.
- [44] B. Zabelich, E. Nitiss, A. Stroganov, and C.-S. Brès, Linear electro-optic effect in silicon nitride waveguides enabled by electric-field poling, *ACS Photonics* **9**, 3374 (2022).
- [45] B. Zabelich, E. Nitiss, A. Stroganov, and C.-S. Brès, Electric-field poling of silicon nitride waveguides for the linear phase modulation, in *Nonlinear Optics and its Applications 2022* (SPIE, 2022), Vol. 12143, pp. 48–54, [10.1117/12.2617189](https://doi.org/10.1117/12.2617189).
- [46] M. M. Fejer, G. Magel, D. H. Jundt, and R. L. Byer, Quasi-phase-matched second harmonic generation: Tuning and tolerances, *IEEE J. Quantum Electron.* **28**, 2631 (1992).
- [47] E. Nitiss, O. Yakar, A. Stroganov, and C.-S. Brès, Highly tunable second-harmonic generation in all-optically poled silicon nitride waveguides, *Opt. Lett.* **45**, 1958 (2020).
- [48] Y. J. Ding, Phase conjugation based on single backward second-order nonlinear parametric process, *Opt. Lett.* **37**, 4792 (2012).
- [49] M. Conforti, A. Locatelli, C. De Angelis, A. Parini, G. Bellanca, and S. Trillo, Self-pulsing instabilities in backward parametric wave mixing, *J. Opt. Soc. Am. B* **22**, 2178 (2005).